Proceedings of the 16th International Conference on Soil Mechanics and Geotechnical Engineering

doi:10.3233/978-1-61499-656-9-2529

Energy analysis and model tests on lateral flow induced by water film effect in liquefied ground

Les essais avec modèles et les analyse de l'approche énergétique sur le mouvement fluctuant par l'effet du film d'eau induit par liquéfaction de la terre

K. Kabasawa & T. Kokusho
Department of Civil Engineering, Chuo University, Tokyo, Japan

ABSTRACT

Considering that water films formed beneath low permeability sublayers in liquefied sand have a great influence on lateral flow mechanism, shaking table tests for saturated sand slopes are carried out. In a saturated uniform sand, flow deformation occurs almost exclusively during shaking, while in a sand slope with a sandwiched silt arc, post-shaking large flow deformation occurs in the upper layer by the water film effect. Results of energy analysis during the post-shaking flow reveal that the shear strength exhibited along the slip surface passing through the water film is only 20 % of that of uniform sand. It takes non-zero value presumably due to the roughness of the slip surface. A close connection has been found between water film induced flow and dilatancy characteristics of sand beneath the low permeability seam.

RÉSUMÉ

Lors du rétablissement d'une liquéfaction du terrain, il semblerait que l'écran d'eau formé par la redistribution des espaces, sous une couche de basse perméabilité, influence grandement le mouvement de fluidité, latéralement., Nous avons alors effectué un essai en banc de vibration après création d'un terrain pentu saturé. En présence d'un terrain sablonneux homogène, le principal mouvement de fluidité survient dès la vibration, alors qu'avec une couche de basse perméabilité, l'écran d'eau génère sur celle-ci un mouvement de fluidité dès la fin de la vibration. Après études réalisées du point de vue énergétique de ces mouvements, la résistance à la force de cisaillement longitudinalement au terrain de basse perméabilité, est de 20% de celle d'un terrain homogène. En outre, par la rugosité de la surface de glissement, la résistance à la force de cisaillement n'a jamais été nulle. Nous avons constaté une corrélation entre le mouvement de fluidité par l'écran d'eau et l'effet de dilatance.

1 INTRODUCTION

There are quite a few damage reports on the lateral flow in liquefied ground in past earthquakes. In some cases, lateral flow occurred not only during but also after earthquakes (Seed, 1987) and flowed more than a few meters even though in very gentle slopes (Hamada et al, 1986). In previous research; Dobry et al (1997), Castro and Poulos (1977) and Meneses et al (1998), lateral flow mechanism was investigated on homogeneous sand.

Generally, a sand deposit is composed of many sublayers in which permeability is different to each other. While it recovers from seismic liquefaction, sedimentation begins in each sublayer. In this process, drained excess pore water may accumulate under a low permeability sublayer. We have named this phenomenon as "water film effect". If the water film is formed continuously beneath the sublayer, the shear resistance along it reduces, having a great influence on lateral flow mechanism. The water film effect was actually demonstrated first by Kokusho (1999) in 1G model tests and later by Malvick et al (2003) in centrifuge tests, too.

In this study, in order to quantify the water film effect on flow failure, 1G model shake table tests have been carried out on a saturated sand slope sandwiching a low permeability seam in it. Based on the test results, the internal friction angle exhibited during the post-shaking flow along the water film is evaluated. Furthermore, the flow mechanism involving water films is discussed from a viewpoint of volume change characteristics of sand observed by CCD cameras.

2 ENERGY ANALYSIS ON LATERAL FLOW INDUCED BY WATER FILM EFFECT

A rectangular lucite soil box with a section of 800mm height, 1100mm width and 600mm thickness (middle size soil box) is filled with water, and fine sand is poured to make a saturated loose sand slope. A arc-shape seam of silt or clay is sandwiched in it as shown in Fig.1. The thickness of the seam is 5mm on average. The grain size curves for the fine sand, silt and clay are available in Fig.2. Their permeability coefficients are 2×10^{-2}

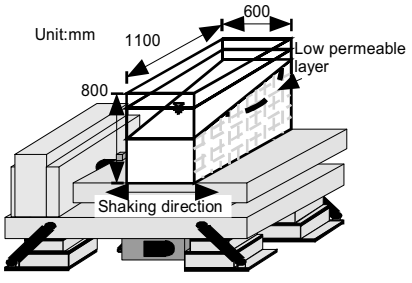

Figure 1. Two dimensional model for saturated sand slope with a silt seam in a lucite box

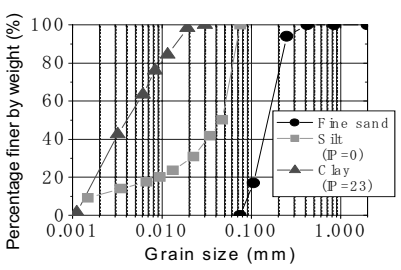

Figure 2. Grain size curves for soil materials used in the tests.

Table 1. Test conditions

	Seam		Rerative density	Acceleration	Slope gradient
	Material	Thickness [mm]	[%]	[gal]	[%]
Case1	---	---	27	290	24
Case2	Silt	3	22	260	25
Case3	Clay	7	22	250	24
Case4	Clay	7	20	300	16
Case5	Silt	3	33	145	24

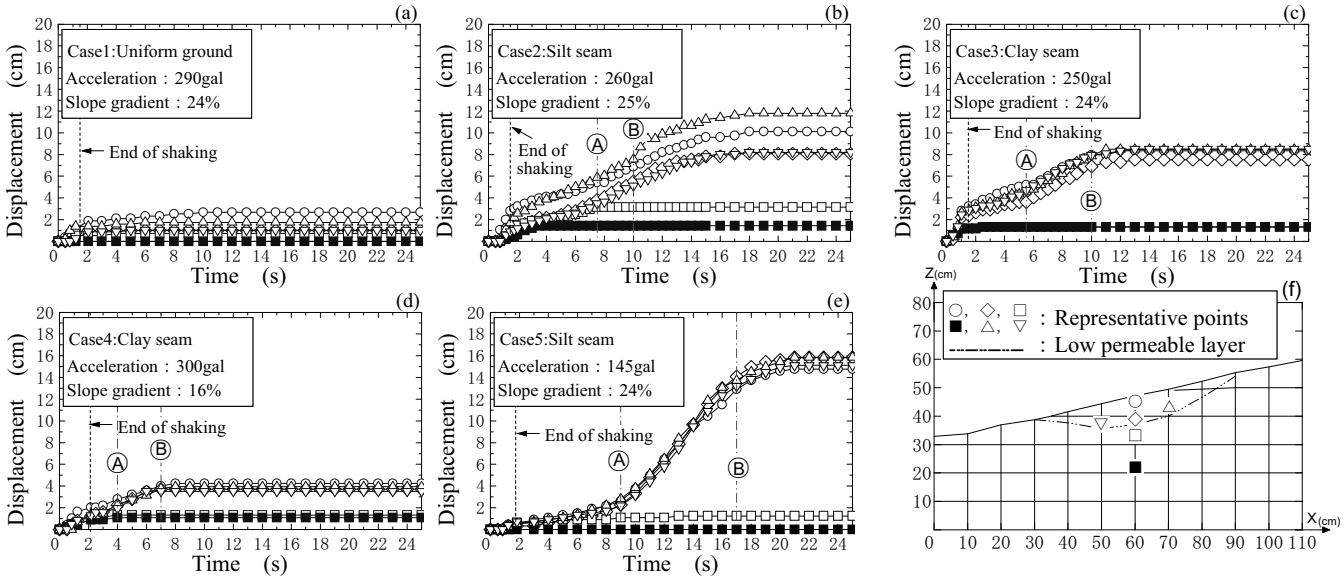

Figure 3. Time histories of displacement of representative points.

cm/s, 2×10^{-4} cm/s and 2×10^{-5} cm/s respectively. The model is liquefied by 3 cycles of cyclic motion in 3 Hz. The direction of shaking is perpendicular to the sloping direction as shown in Fig.1 so that the effect of the inertia force be excluded in the lateral flow deformation. In these tests, failure modes are visualized by movements of marker grids made from Japanese noodles attached to the transparent wall of the soil box. Test conditions are shown in Table 1. Tests for slopes of uniform sand are also carried out to compare with those sandwiching a silt seam.

Displacement time histories of representative points designated in Fig.3 (f) are shown in Fig. 3 (a)~(e). In Case 1 without a seam, major displacement occurs mostly during shaking, while in other cases with a seam, larger flow displacement occurs during shaking. Water film can be observed beneath the seam that enables upper sand mass to move discontinuously along the silt seam even after shaking.

In Cases 2 ~5, the residual shear strength exerted along the water film during the flow is calculated by the energy balance of the upper sand mass above the water film. In Fig.3 (b)~(e), the potential and kinetic energies at A and B are denoted as $E_{PA,}$ E_{KA} and $E_{PB,}$ $E_{KB,}$ respectively. In addition, the energy loss by friction between A and B is denoted as W. Therefore the energy balance is expressed as follows;

$$(E_{PA}-E_{PB})+(E_{KA}-E_{KB})=\triangle E_P+\triangle E_K=W \tag{1}$$

Eq. (1) indicates that the change in the potential energy and the kinetic energy is equal to the energy loss during the flow between A and B.

In order to numerically evaluate Eq. (1), the upper sand layer is divided into n (n=6) segments. For each segment, the height of the center of gravity h_i of i'th segment is measured from video pictures at small time increments. Then, the potential energy change is evaluated from the change in h_i, buoyant mass M_i' and the acceleration of gravity g for each block. Consequently, the change of potential energy between A and B is formulated as;

$$\triangle E_P=\sum_{i=1}^{n}M_{Ai}'gh_{Ai}-\sum_{i=1}^{n}M_{Bi}'gh_{Bi} \tag{2}$$

Similarly, the change in the kinetic energy is expressed as

$$\triangle E_K=\frac{(\sum_{i=1}^{n}M_{Ai}v_{Ai}^{\,2}-\sum_{i=1}^{n}M_{Bi}v_{Bi}^{\,2})}{2} \tag{3}$$

where v_i = the velocity of the soil mass M_i in the i'th segment.

It is assumed here that energy loss W in Eq. (1) between Point A and Point B consists of W_1 to W_3, where W_1 = energy loss by friction along the water film, W_2 = the energy loss by the friction between the sand and the side walls of the box and W_3 = the energy loss by viscosity of water in the water film. They are expressed as;

$$W_1=\tan\phi's\sum_{i=1}^{n}(\sigma_i'\cos\theta_iA_i) \tag{4}$$

$$W_2=s\sum_{i=1}^{n}2\frac{\delta_i'}{2}l_i\mu K_0B_i \tag{5}$$

$$W_3=\mu_W\frac{\Delta v_{Aav}}{\Delta d}s\sum_{i=1}^{n}A_i \tag{6}$$

Table 2. Results of energy analysis

	Displacement s [cm]	Energy increment ΔE [J]	$\Sigma A_i \sigma_i \cos\theta_i$ [N]	W_2 (J)	Calculated internal friction angle of sand ϕ' [deg]
Case2	0.0179	0.34	1.95	0.072	7.8
Case3	0.0308	0.82	4.91	0.158	7.7
Case4	0.0176	0.25	2.08	0.044	5.7
Case5	0.1250	2.45	26.88	0.803	3.5

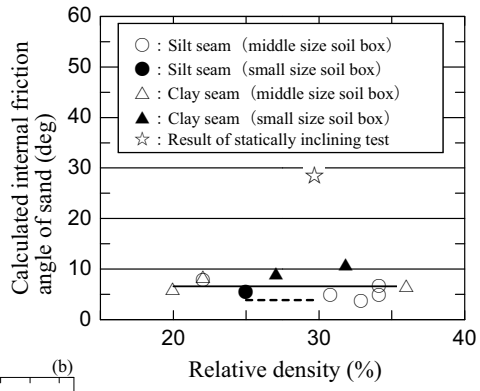

Figure 4. Relative density versus calculated internal riction angle

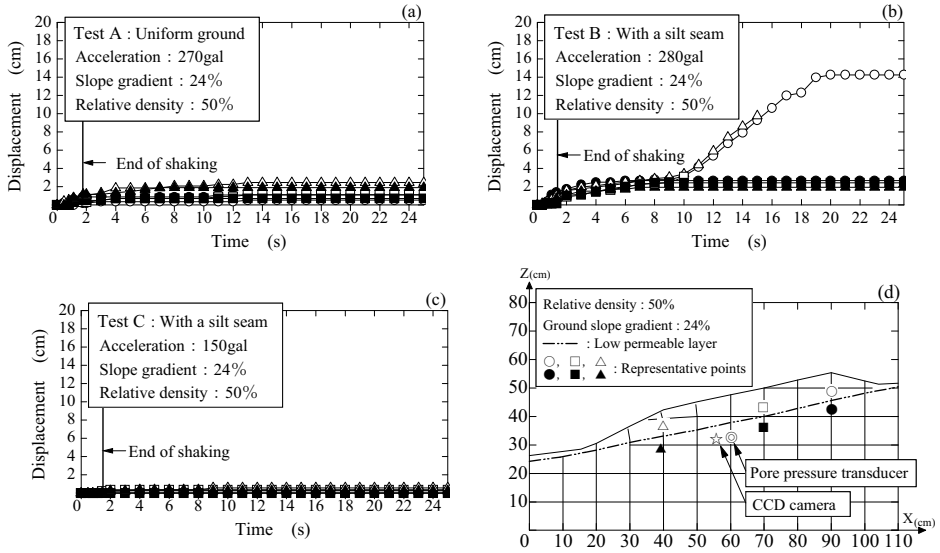

Figure 5. Time histories of deformation and location of representative points (Test A ~C)

respectively, where ϕ' = the equivalent friction angle in terms of effective stress, σ_i' = effective stress, θ_i = the gradient of the slip surface, A_i = the area of the slip surface, l_i = the segment height and B_i = the segment width, in the i'th segment respectively. The friction coefficient between sand and both sides of the acrylic soil container μK_0 is assumed as 0.125 based on a tube test carried out by Kokusho and Kojima (2002). The viscosity coefficient of water μ_w is assumed 1.307 mPa, and the thickness of water film d is assumed 0.1mm. The flow displacement s and average velocity of soil mass v_{av} tangent to the slip surface are assumed constant along the surface because the soil mass rotates along the slip surface almost as a rigid block.

Then, Eq (1) is expressed as

$$\Delta E_P + \Delta E_K = W_1 + W_2 + W_3 \tag{7}$$

The equivalent internal friction angle ϕ' in terms of effective stress between Point A to B can be calculated backward from Eq. (7).

Fig.4 shows a relationship between the equivalent friction angle and the relative density obtained from a series of similar model tests with the two type of seams, silt or clay, using two different soil boxes. The star symbol indicates the angle of repose, ϕ' =29 degrees, measured by a static test in which the same slope of the homogeneous sand is inclined (Kabasawa and Kokusho,2001). Fig.4 indicates that the average equivalent friction angle is 6.6 degrees, and the residual strength decreases to about 20% of that for a homogeneous slope. In spite of the differences in the test conditions such as the relative density of sand, the plasticity of the seam, the model size, etc. the residual strength along the slip surface beneath seam is almost the same.

The broken line in Fig.4 indicates the equivalent friction angle obtained in a different series of model tests (Kabasawa and Kokusho, 2004) on slopes including a straight seam parallel to ground slope and trapezoidal upper soil mass ensuring free down-slope flow [See. Fig.5 (d)]. In that case, the average equivalent friction angle is 3.9 degrees, and the residual strength decreases further down to about 10% of that for a homogeneous slope. The difference in the reduction of equivalent friction angle may possibly be explained by the difference in the configuration of the slip plane.

It should be noted, here, that in the two series of tests the equivalent friction angle is evaluated as non-zero value. The non-zero strength cannot be explained if the slip surface actually passes all through continuous water film. In order to clarify the reasons, microscopic observation on volume change characteristics in sand below the seam is carried out as follows.

3 DILATANCY EFFECT OF SAND ON LATERAL FLOW INVOLVING WATER FILMS

Now, there may be a question that if shear strain of sand beneath a silt seam increases with increasing lateral flow in the upper sand layer, the water film would be absorbed by the dilation of the sand skeleton, prohibiting the formation of a

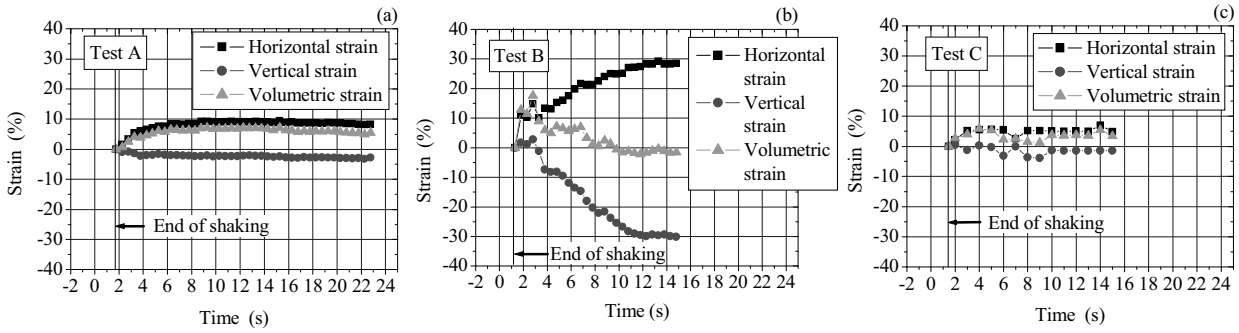

Figure 6. Time histories of strain (Test A ~ C)

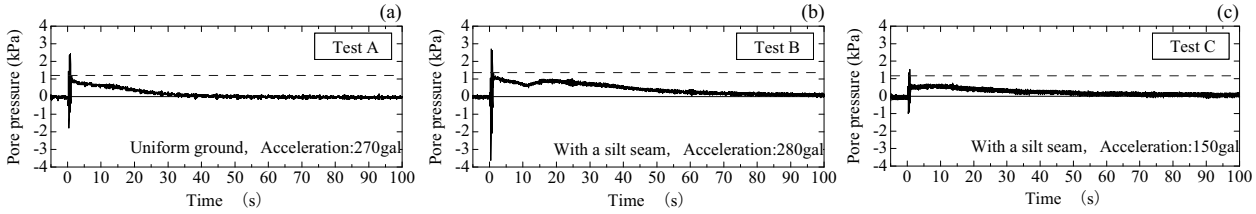

Figure 7. Time histories of pore pressure (Test A ~ C)

continuous water film. In order to discuss this problem based on the experimental facts, it is essential to know the volume change of sand beneath the seam after the end of shaking. Therefore, volume change is measured in some of the model tests by using CCD cameras. The locations of the cameras are indicated in Fig.5 (d). In video images through the transparent side wall, representative sand grains with peculiar colors are chosen as markers and there post-shaking flow movements are traced. By combining those markers, it is possible to calculate normal and shear strain in terms of horizontal and vertical axes. The volumetric strains are calculated as a sum of the vertical and horizontal strains.

Fig.6 shows time histories of the horizontal and vertical strains and the volumetric strains. In Test A, without a low permeable seam, the amount of deformation is very limited and occurs mostly during shaking [See. Fig.5 (a)]. The volumetric strain shows expansion presumably because of dilatancy effect due to static shear stress loaded by the slope, leading to the decrease in pore water pressure after shaking [See. Fig.7 (a)].

On the other hand, in Test B with a silt seam, the horizontal strain and vertical strains both increases, resulting in maximum volume expansion a few seconds after shaking. However, as the amount of flow increases, the volumetric strain changes into contraction after 10 seconds, which corresponds to the beginning of the flow due to water film [See. Fig.5 (b)]. In spite of large lateral flow, the dilation of the sand is not observed in Fig.6 (b) and the pore pressure there increases again [See. Fig.7 (b)], though it is still smaller than the effective overburden shown with the dashed line in the chart. This is because the shear stress doesn't transmit to the sand underneath through the water film and the volumetric strain remains almost constant due to shear stress isolation effect (Kokusho, 2000). In Test C with a silt seam and small amplitude shaking, lateral flow does not occur as shown in Fig.5 (c). Volumetric strain maintains the expansion side all the time. For this reason, migrated water is absorbed in the expanded sand and the water film cannot be formed.

It may be inferred from these test results that the reason why the residual strength cannot be completely zero is somehow related with the combination of water supply rate and volume change rate due to increasing shear strain during flow deformation. More research is certainly needed to quantitatively clarify the mechanism of residual strength mobilization along the water film.

4 CONCLUDING REMARKS

Model tests, energy analyses and CCD camera observation have yielded the following major conclusions;

1) Residual strength along the slip surface beneath a low-permeability seam considerably decreases to about 20% or 10% of that of homogeneous sand for model tests of an arc-shaped seam and straight seam, respectively.
2) In spite of the difference in test conditions such as the relative density of sand, etc., the residual strength along the slip surface beneath the seam is almost the same non-zero value, indicating a dominant effect of the water film.
3) When the post-shaking volumetric strain induced by static shear stress changes into contraction, pore pressure increases and lateral flow of the upper soil mass occurs along a water film. In contrast, when volumetric strain maintains expansion side, water film is not formed.
4) It is estimated that the non-zero residual strength is somehow related with the time-dependent rate of pore water supply and soil dilatancy due to shearing.

REFERENCES

Castro, G. and Poulos, S.J. 1977. "Factors affecting liquefaction and cyclic mobility." *Journal of Geotechnical Engineering,* Vol.103, No.6, 501-516.

Dobry, R., Taboada, V., Liu, L. 1995. "Centrifuge modeling of liquefaction effects during earthquakes." *Proc. of 1st International Conference on Earthquake Geotechnical Engineering, ASCE,* Vol.3, 1291-1324.

Hamada, M., Yasuda, S., Isoyama, R. and Emoto, K. 1986. "Observation of permanent ground displacements induced by soil liquefaction" *Journal of Geotechnical Engineering, Japan Society of Civil Engineers,* No.376, Ⅲ-6, 211-220, (in Japanese).

Kabasawa, K. and Kokusho. T. 2001. “Possibility of water film generation in saturated sand slope subjected to static loading.” *Proc. Annual Convention of Japan Society of Civil Engineers*, Vol.3, 346-347, (in Japanese).

Kabasawa, K. and Kokusho. T. (2004). “Model test and energy analysis on lateral flow by water film effect in liquefied sand slope including silt seam.” *13th .WCEE. Canada.,* No.340.

Kokusho, T. 1999. “Water film in liquefied sand and its effect on lateral spread., *Journal of Geotechnical and Geoenviromental Engineering, ASCE*, Vol.125, No.10, 817-826.

Kokusho,T. 2000.: Mechanism for water film generation and lateral flow in liquefied sand layer, Soils and Foundations, Vol.40, No.5, pp.99-111.

Kokusho,T. and Kojima,T. 2002. “Mechanism for Postliquefaction Water Film Generation in Layered sand.” *Journal of Geotechnical and Geoenviromental Engineering, ASCE*, Vol.128, No.2, 129-137.

Malvick, E. J., Kulasingam, R., Boulanger, R. W., & Kutter, B. L. 2003 Analysis of a void redistribution mechanism in liquefied soil. *Proc. 12th Panam Conf. Soil Mech. & Geotech. Engrg,* Cambridge, MA. Vol. 2, pp. 955-961.

Meneses, J., Ishihara, K., Towhata, I. 1998. “Effects of superimposing cyclic shear stress on the undrained behavior of saturated sand under monotonic loading.” *Soil and Foundations,* Vol.38, No.4, 115-127.

Seed, H. B. 1987. “Design problems in soil liquefaction.” *Journal of Geotechnical Engineering, ASCE,* Vol.113, No.8, 827-845.